



TECHNICAL ARTICLE

Fabrication of Al/Mg Bimetallic Thin-Walled Ultrafine-Grained Tube by Severe Plastic Deformation

S.M. Hosseini, M. Roostaei, M. Mosavi Mashhadi, H. Jabbari, and G. Faraji

Submitted: 3 August 2021 / Revised: 8 November 2021 / Accepted: 21 November 2021 / Published online: 20 January 2022

Multilayer composites have recently attracted considerable attention due to their ability to take advantage of the benefits of various metallic materials simultaneously. The present study is the first to use parallel tubular channel angular pressing (PTCAP) as a severe plastic deformation method to fabricate a bimetal Al/Mg tube. This process was applied on commercially pure aluminum along with an AM60 magnesium alloy at the temperature range of 250–400 °C. According to the microstructural and mechanical tests, there is a strong bond between layers besides the grain refinement after the process. Additionally, microhardness examinations showed that there is an excellent homogeneity in addition to the dramatic increase in the hardness of bimetallic PTCAP processed Al/Mg tube. Scanning electron microscope and energy-dispersive x-ray spectroscopy analyses in the interface between the layers and also the results of the shear strength test showed that by increasing the temperature, the diffusion rate at the interface increases. For instance, the significant bonding strength of 30 MPa was achieved after the PTCAP specimen at 400 °C. Therefore, these investigations substantiate that the PTCAP process can be used as an appropriate cladding technique for obtaining simultaneous severe plastic deformation microstructures and sufficient bonding strength in the production of bimetallic tubes.

Keywords bimetallic tube, microstructure, nanocrystalline material, severe plastic deformation, thin-walled tube

1. Introduction

In recent years, magnesium and its alloys have flourished in the aerospace and automotive industry due to their special properties, such as high strength-to-weight ratio, good castability, and high thermal and electrical conductivity (Ref 1–3). While magnesium has been used extensively, there are limits to its use due to its poor ductility, which can be attributed to its hexagonal closed packed (hcp) crystal structure and limited slip systems at the ambient temperature, and its low corrosion resistance (Ref 4–6). Regarding corrosion properties, there is no self-healing passivation layer for magnesium, rendering it highly vulnerable to galvanic attack (Ref 7). One of the successful methods to overcome these drawbacks is to fabricate multilayered composite materials. Recent studies have shown that combining various materials can effectively optimize mechanical properties, corrosion, and abrasion resistance while decreasing total weight (Ref 1–4). Among the materials to combine with Mg alloys, Al and its alloys are excellent candidates. In fact, proper corrosion resistance and better

ductility of aluminum alloys have made them suitable candidates for magnesium coatings (Ref 8). Thus, magnesium/aluminum bimetallic products have attracted considerable attention.

Several methods have been proposed for cladding dissimilar metals, which can be classified into two general groups based on their nature. First, their focus mainly is on bonding of layers, namely roll bonding (Ref 9), diffusion bonding (Ref 10), explosive welding (Ref 11, 12), friction stir welding (Ref 13, 14), extrusion (Ref 15), twin roll casting (Ref 16), casting (Ref 17, 18), hot pressing (Ref 19), cold rolling (Ref 20), and transient liquid phase (TLP) (Ref 21). Besides, the second group's approaches focus on the bonding of layers and grain refining of metals simultaneously, including SPD-based methods such as accumulative roll-bonding (ARB) (Ref 22). SPD techniques are among the most effective methods to produce multilayered components. In fact, they are able to clad dissimilar materials while imposing very high strain on materials, leading to the production of ultrafine-grained materials (Ref 23).

Recently, researchers have put much effort into developing complicated components, notably multilayered tubes. Consequently, their effort resulted in some proper approaches based on the SPD-based process and the fundamentals of cladding the tubular components. Some well-known SPD processes used for processing tubular bimetallic components are as follows: high-pressure tube twisting (HPTT) (Ref 24), tube extrusion shearing (TES) (Ref 25), equal channel angular pressing (ECAP) (Ref 26), accumulative extrusion bonding (AEB) (Ref 27). The methods mentioned above have some drawbacks, including poor bonding strength, requiring advanced equipment, and low microstructural homogeneity through the materials. We conduct a new method to produce ultrafine-grained multilayer tubular components based on the PTCAP method to overcome these

S.M. Hosseini, M. Mosavi Mashhadi, H. Jabbari, and G. Faraji, School of Mechanical Engineering, College of Engineering, University of Tehran, 11155-4563, Tehran, Iran; and **M. Roostaei**, School of Metallurgy and Materials Engineering, College of Engineering, University of Tehran, P.O. Box 11155-4563, Tehran, Iran; and Erich Schmid Institute of Materials Science, Austrian Academy of Sciences, 8700 Leoben, Austria. Contact e-mail: ghfaraji@ut.ac.ir.

drawbacks. The PTCAP process was introduced by Faraji et al. as a suitable method to produce single-layer ultrafine-grained tubes (Ref 28, 29). Since then, this method has been used to process many materials, all of which were single-layer tubes. The PTCAP has been used to enhance single-layer tubes' mechanical properties through severe plastic deformation with a low required force and homogenous strain distribution (Ref 30-33). Based on this research work, the PTCAP process allows for the fabrication of multilayered tubes with less required force and better bonding strength between layers without requiring special equipment, while the tubes become ultrafine-grained, resulting in a considerable improvement in the mechanical properties of the materials.

The PTCAP process for tube cladding consists of two half-cycles. As illustrated in Fig. 1, in the first half-cycle, the upper punch presses the tubes through the gap between the mandrel and the die. After passing through the shear zone, the tubes reach their maximum size in the first half cycle (Fig. 1a). In the second half-cycle, the double-layered tube with an increased size was pressed back by the lower punch into the shear zone again. The tube will reach its initial size by completing this step, as illustrated in Fig. 1(b). In other words, the PTCAP process is able to fabricate bimetallic tubes with excellent bonding strength and superior mechanical properties, while there would be no change in the final geometrical dimensions of the specimens.

The total accumulative strain $\bar{\epsilon}_T$ in the first half cycle of the PTCAP processing can be calculated using the following equation (Ref 28), which is derived from the common engineering formulae as well as the geometry presented in Fig. 2(a)

$$\bar{\epsilon}_T = \sum_{i=1}^2 \left[\frac{2\cot(\varphi_i/2 + \psi_i/2) + \psi_i \operatorname{cosec}(\varphi_i/2 + \psi_i/2)}{\sqrt{3}} \right] + \bar{\epsilon}_\theta$$

where φ and ψ are the angles of the channel and curvature, respectively.

$$\bar{\epsilon}_\theta = \frac{2}{\sqrt{3}} \epsilon_\theta$$

$$\epsilon_\theta = \ln \frac{R_2}{R_1}$$

where the R_1 and R_2 are shown in Fig. 2.

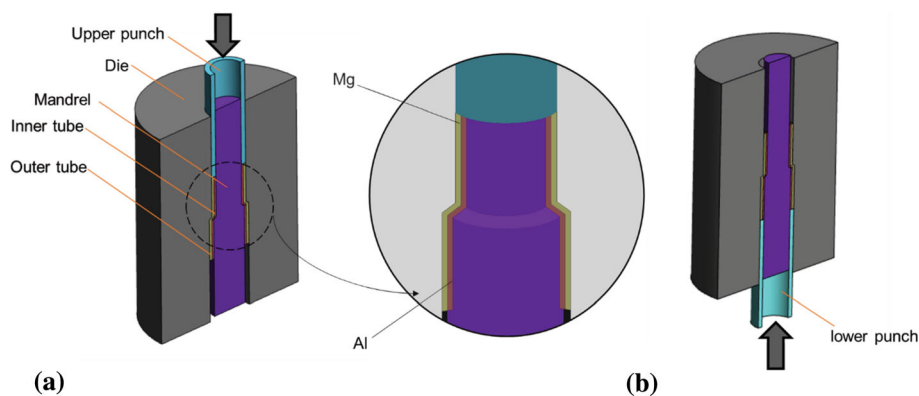


Fig. 1 Schematic of the PTCAP process (a) first-half pass, (b) second-half pass

After N passes, the total equivalent strain can be estimated by the following equation (Ref 28):

$$\bar{\epsilon}_{TN} = 2N \left\{ \sum_{i=1}^2 \left[\frac{2\cot(\varphi_i/2 + \psi_i/2) + \psi_i \operatorname{cosec}(\varphi_i/2 + \psi_i/2)}{\sqrt{3}} \right] + \bar{\epsilon}_\theta \right\}$$

Although the Al/Mg bimetallic tube plays a vital role in industries, particularly those exposed to a chemical environment, most cladding techniques were applied to Al/Cu components. Therefore, this paper presents the first application of the PTCAP method to fabricate Al/Mg (commercially pure aluminum and magnesium alloy AM60). It is noteworthy that the article focuses mainly on the Mg layer since the AM60 component has a more complicated microstructure than the Al component.

2. Experimental Procedure

The experimental materials consisted of as-cast magnesium AM60, which contains 5.65% Al, 0.24% Zn, 0.27% Mn, 0.07% Si, 0.01% Cu, 0.004% Fe, 0.003% Ni (all expressed in wt.%) for the outer tube and sheet-formed pure aluminum 1050 for the inner one. The inner tube (Al1050) with an outer diameter of 17 mm, a thickness of 1 mm, and a length of 400 mm was precisely cut through a wire cut machine. The outer tube (AM60) with 20 mm in outer diameter, 1.5 mm in thickness, and 40 mm in length was also cut through the wire-cut electro-discharge machine for better accuracy in size. Figure 3 illustrates the specimens before and after the PTCAP process. Then, all specimens were annealed at 350 °C for 2 h prior to the processing in order to obtain a homogeneous microstructure. The die, the mandrel, and the punches were manufactured from H13 hot-worked die steel and subsequently were hardened up to 55 HRC. The die parameter, which is illustrated in Fig. 2(a), is presented in Table 1.

To reduce friction, molybdenum sulfide (MoS_2) was sprayed on all surfaces involved in the PTCAP process, except the interface between Al and Mg. Al and Mg tubes were fitted together through the sliding fit. Afterward, Al/Mg tubes were PTCAPed at temperatures of 250, 300, 350, and 400 °C with 10 mm/s ram speed. Vickers microhardness was conducted at a transverse cross section of the Al/Mg tubes using the Coopa model microhardness machine at a load of 50 gr applied for 15 s.

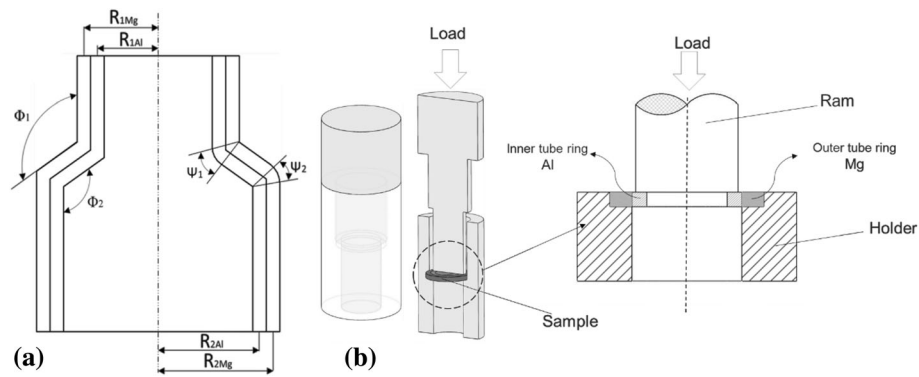


Fig. 2 (a) Die parameters diagram, (b) schematic of shear bond test

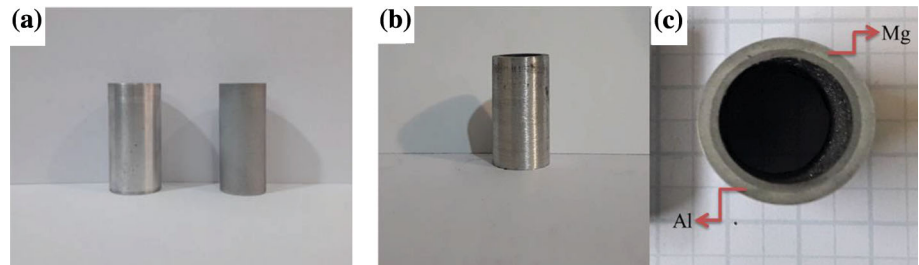


Fig. 3 The specimens, (a) before the process, (b), and (c) after PTCAP processing

Table 1 The die parameter's value

Parameter	R_1 (Al)	R_1 (Mg)	R_2 (Al)	R_2 (Mg)	Channel angle (ϕ_1, ϕ_2)	Curvature angle (ψ_1, ψ_2)	Total equivalent strain
Value	8	9.25	10.5	11.75	120°	0°	AM60 2.5
...	Al1050 3.28

For characterization, the specimens were polished and etched with a solution containing 4.2 gr pitric acid, 70 ml ethanol, 10 ml acetic acid, and 10 ml distilled water. Then, optical microscopy was used in order to investigate the microstructure of the AM60 surfaces at a transverse cross section of tubes. Furthermore, the surfaces of the Al1050 in the bimetallic tubes were also polished and electro-etched for optical microscopy. Measurements of grain size are conducted using the linear intercept method according to the ASTM E112-13 standard. The PTCAPed AM60 layer at various temperatures was also characterized by the scanning electron microscope (SEM) using the FEI NOVA NANOSEM 450 model machine. The phase constitutions of the AM60 layers of each specimen were analyzed using an x-ray diffraction analysis with Cu $K\alpha$ radiation by the PHILIPS PW1730 machine. The chemical compositions of the AM60 tube were detected by an SEM equipped with an energy-dispersive x-ray spectroscopy (EDS) analysis. Furthermore, the microstructure of Mg layers was analyzed by the transmission electron microscope (TEM) model FEI Tecnai G2 F20 SuperTwin at 20KeV. The samples for the TEM analysis were cut $2 \times 2 \times 0.1$ mm from Mg layers, which was PTCAPed at the 300 and 400 °C. The samples were prepared by double jet polishing using 50 cm^3 perchloric acid, 25 cm^3 2-butoxyethanol, 450 cm^3 ethanol solution at 230-240 K, 8-10 V.

Additionally, the shear bond test was performed in order to investigate the bond strength between the two layers of each

specimen at room temperature (Fig. 2b). All samples for the mentioned test were cut with a length of 2 mm in the transverse cross section direction (TD). A load with a constant ram speed of 0.5 mm/min at the ambient temperature was applied continuously until the specimens were failed. The shear bond strength was calculated by the following equation.

$$\sigma_t = \frac{F_{\max}}{A} = \frac{F_{\max}}{\pi dh}$$

where σ_t is the bond strength, F_{\max} is the maximum compression force, A is the area of the shear plane, d is the diameter of the interface, and h is the ring thickness.

3. Results and Discussion

3.1 Microstructure

The microstructure of the as-cast AM60 Mg alloy after annealing at 350 °C for 2 h is shown in Fig. 4(a). The microstructure contains coarse grains of the α -Mg phase with an average linear intercept length of 300 μm and isolated particles of intermetallic β -phase ($\text{Mg}_{17}\text{Al}_{12}$). The eutectic β -phase ($\text{Mg}_{17}\text{Al}_{12}$) in the as-cast microstructure is generally distributed in grain boundaries (GBs) as a network-like

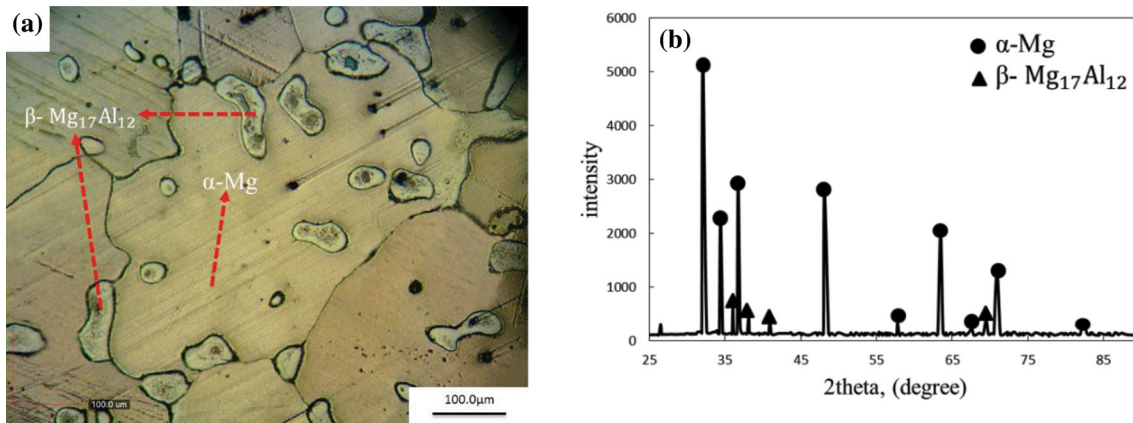


Fig. 4 (a) Optical micrographs and (b) XRD pattern for AM60 magnesium alloy after annealing at 350 °C for 2 h

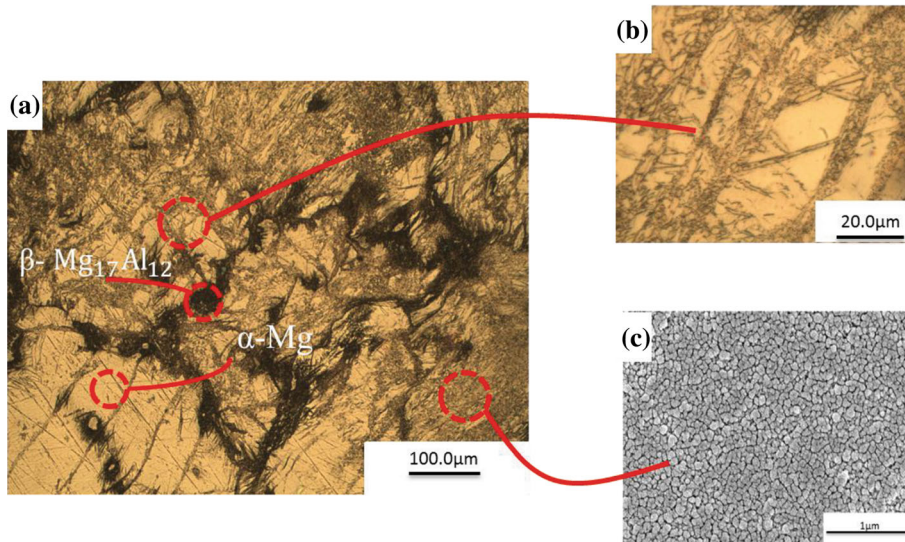


Fig. 5 (a) and (b) Optical micrographs and (c) SEM image after one pass of PTCAP at the temperature of 250 °C for AM60 magnesium alloy

structure that reduces the strength of Mg alloy (Ref 34). On the other hand, although the heat treatment at high temperature ($T > 400\text{ °C}$) for a long time causes the dissolution of the coarse β -phase network, that process is time-consuming and has drawbacks such as grain growth and oxidation. According to previous research, based on the improvement of ductility, the annealing around solvus line for a short time has caused the conversion of β -phase network structure to the isolated particles via partial dissolution (Ref 35). As can be seen in Fig. 4(a), this phase is distributed along the GBs as isolated particles, and its presence after annealing was subsequently verified by XRD patterns as shown in Fig. 4(b).

AM60 alloy's optical micrograph after one pass of PTCAP at the temperature of 250 °C is displayed in Fig. 5(a). As it is seen, remarkable grain refinement happened by dynamic recrystallization (DRX), developed broadly along initial GBs, in the regions with precipitates near the original GBs, inside and on boundaries of twins (Fig. 5a and b). Due to the storage of high energy in the course of deformation, twins are favorable sites for nucleation of new grains (Ref 36); hence, twinning plays a crucial role in low-temperature deformation. Bimodal distribution of grains and undissolved $\text{Mg}_{17}\text{Al}_{12}$ phases are

visible in the structure, and the SEM image shows that the grain size in some recrystallized regions reaches $\sim 0.1\ \mu\text{m}$ (Fig. 5c).

In order to investigate the effect of process temperature on microstructure, the representative microstructure of PTCAPed AM60 alloy at temperatures of 300 and 400 °C is shown in Fig. 6(a) and (c). As shown by the results, due to the operation of the non-basal slip systems, no twinning can be found at the high deformation temperature of 300 and 400 °C and microstructures composed of large unrecrystallized zones surrounded by the fine-grained DRX necklace structure. The necklace structure is a typical microstructure in Mg alloys after deformation at high temperatures so that with the progress of deformation, DRX sets in the bulged GBs, and gradually the initial grains are replaced with equiaxed DRX grains, which are formed as a necklace along the initial GBs (Ref 37, 38). In addition, metallographic observations reveal that with the increasing temperature of deformation, a fraction of DRX was enhanced. When the PTCAP temperature was higher than 350 °C, the homogenous microstructure appeared due to full crystallization. The grain size distribution histograms for the AM60 section of the tubes PTCAPed at temperatures of 300 °C and 400 °C are presented in Fig. 6(a) and (c). As it can be seen, the average primary grain size of about 300 μm was refined to

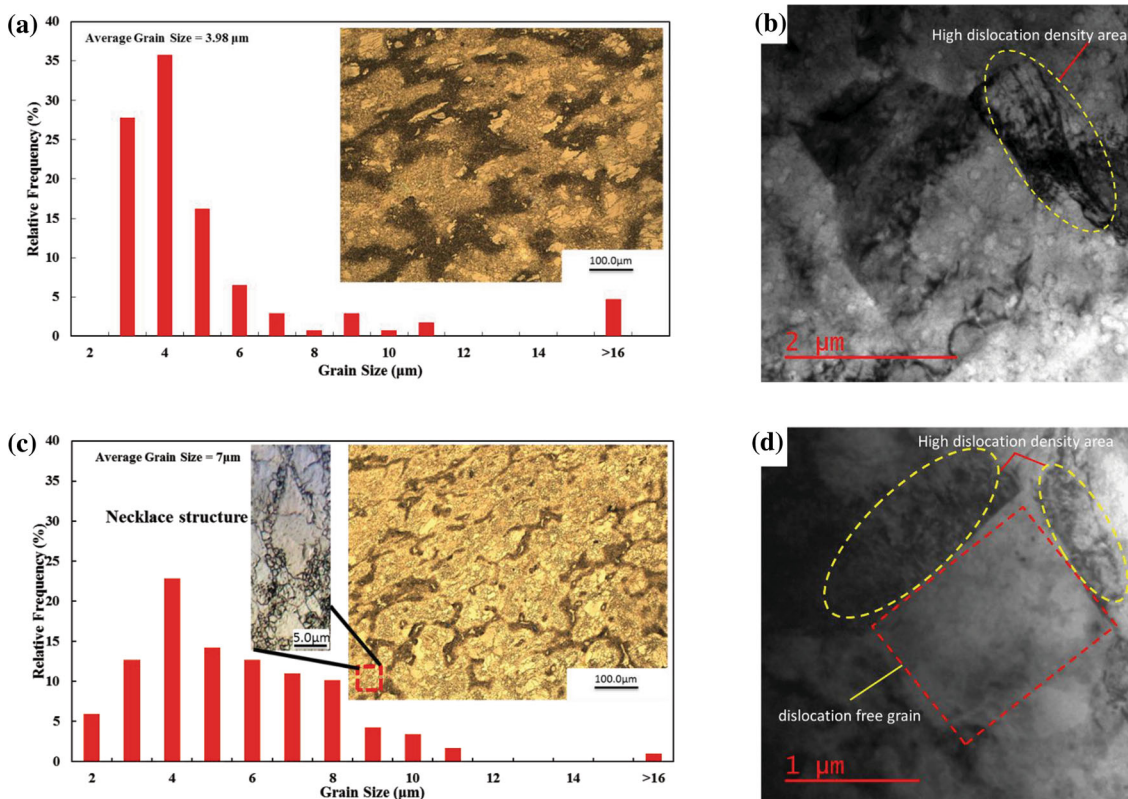


Fig. 6 Optical micrograph, grain size distribution histogram, and TEM bright-field image of PTCAPed AM60 alloy at a temperature of (a, b) 300 °C, and (c, d) 400 °C

about 3.98, and 7 μm after one pass of PTCAP at 300, and 400 °C, respectively. Increasing the average grain size and moving the grain size distribution histograms toward coarser recrystallized grains by increasing PTCAP temperature can be attributed to the further activity of non-basal slip systems, dynamic restoration mechanisms, and limited grain growth processes. These results are in good agreement with other reports regarding the microstructure evaluation of AM60 alloy (Ref 34).

TEM images from the transverse section of samples PTCAPed at 300 and 400 °C (Fig. 6b and d) show the high density of dislocation in microstructure, although some grains are free of dislocations. Observations have shown that as the temperature rises, the number of free dislocation's grains increases. Sharp grain boundaries without any considerable wavy shape can be seen in sample PTCAPed at 400 °C as well. This may be linked to restoration phenomena and the consequent low magnitude of dislocations density.

As can be seen in Fig. 7(a), (b), and (c), besides the DRX, dissolution and fragmentation of $Mg_{17}Al_{12}$ phases simultaneously occur in the PTCAP process in AM60 alloy. In other words, during the PTCAP process, the previous β -phase was broken down and distributed along the newly formed DRX grain boundaries and inside the grains. Figure 7(a), (b), and (c) shows the distribution of this phase after the PTCAP process at temperatures of 250, 350, and 400 °C. The crushed precipitates, like pinning obstacles, can prevent grain growth, which limits the growth of DRX grains. By increasing PCAP temperature ($T > 350$ °C), the amount of pinning precipitates decreases due to the dissolution of β -phase, and the DRX grain size becomes larger. In fact, the dissolution of β -phase and consequently the

slight growth of grains at temperatures above 350 °C are one of the factors contributing to the increase in the average grain size. It should be noted that the EDS analysis of precipitates demonstrated that the Mg/Al ratio of $Mg_{17}Al_{12}$ phases is slightly higher than the stoichiometric composition ratio, 1.42, and a similar phenomenon has been reported by Zhao et al. (Ref 39) (Fig. 7d). The excessive Mg content in the spectrum could be due to the excess Mg by the α -Mg solid solution matrix. TEM analysis of the PTCAP samples processed at 350 °C (inserted in Fig. 7b) and 400 °C (not shown) demonstrated that the $Mg_{17}Al_{12}$ precipitates have relatively oval morphology, although irregularly shaped precipitates are also clearly found in the microstructure. The size of the β - $Mg_{17}Al_{12}$ precipitate ranges from 0.2 to 1 μm in both samples; however, with increasing temperature, the size distribution shifts to smaller sizes.

Although a detailed study of the microstructure of Al is not included in this study, the optical images of the microstructure show that the PTCAP technique also leads to a significant refinement in the microstructure of the Al layer by recrystallization of the microstructure. As a result, after one pass of PTCAP at 350 °C, the as-annealed microstructure of Al with an average grain size of 200 μm is reduced to 70 μm (Fig. 8b).

3.2 Microhardness

As shown in Fig. 9, the hardness of the initial Al and AM60 tubes has increased dramatically after a pass of the PTCAP process. The Al layer's average hardness has risen from 31 to 49 Hv, and the average hardness of the Mg layer has increased from 67 to 105 Hv after a pass PTCAP at 250 °C. According to

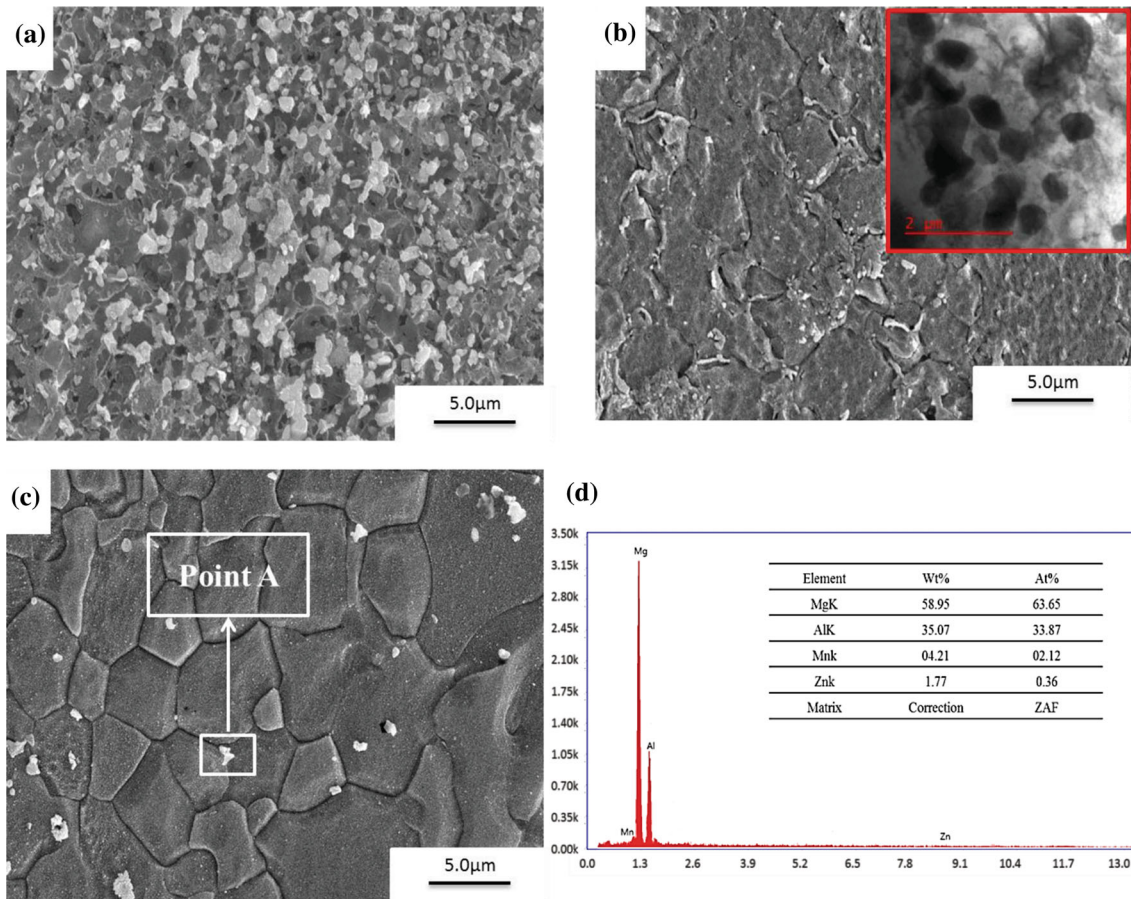


Fig. 7 SEM image of PTCAPed AM60 alloy at a temperature of (a) 250 °C, (b) 350 °C, (c) 400 °C, and (d) EDS patterns of point A in (c)

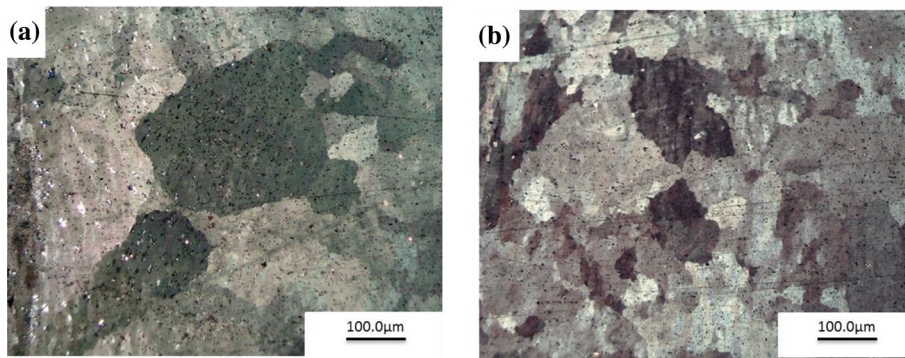


Fig. 8 Optical micrograph of Al1050 alloy (a) annealed (b) PTCAPed at 350 °C

the Hall–Petch equation, there is a general agreement that the mechanical properties of metals, such as hardness, depend on their grain size (Ref 40). Therefore, the considerable decrease in grain size stemmed from the PTCAP process is the main reason for increasing the hardness in both layers. Al 1050 with an initial grain size of between 200 μm and 300 μm after two passes of equal channel angular extrusion (ECAE) at room temperature shows roughly the same hardness compared to specimens PTCAPed at 250 °C (Ref 41). The higher equivalent plastic strain values in the PTCAP method (~ 3.2) are the key factor for this method's advantage over ECAE. As displayed in Fig. 9, by increasing PTCAP temperature from 250 to 400 °C, the average hardness of Al and AM60 sections decreased. This

phenomenon can be explained by the occurrence of softening processes in the deformed structure, which are controlled by the rate of dynamic recovery. For AM60 alloy, the abatement of hardness for the temperature increasing from 300 to 350 °C is about 9% and ~ 20% for the temperature enhancement from 350 to 400 °C. According to the microstructural study of the previous part, one of the other factors to justify this sudden drop in microhardness is probably related to the dissolution of β-phase and subsequent grain growth. In order to determine the level of homogeneity of the samples, the Vickers microhardness was measured across the cross sections of the tubes processed by PTCAP. Figure 10(a) schematically shows the distribution of microhardness points in cross sections of the PTCAPed

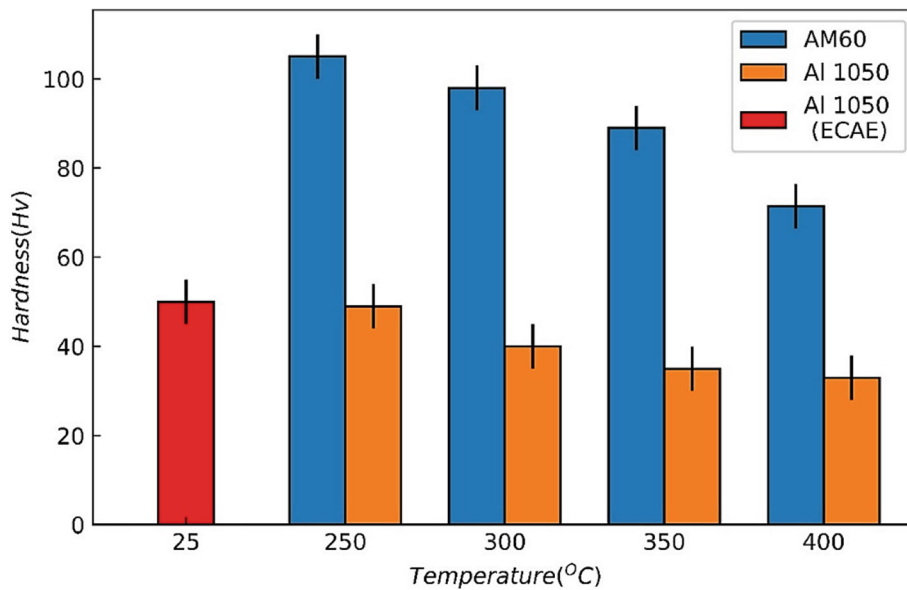


Fig. 9 Microhardness (Hv) of AM60 Mg alloy and Al1050 after one pass of PTCAP at different temperatures

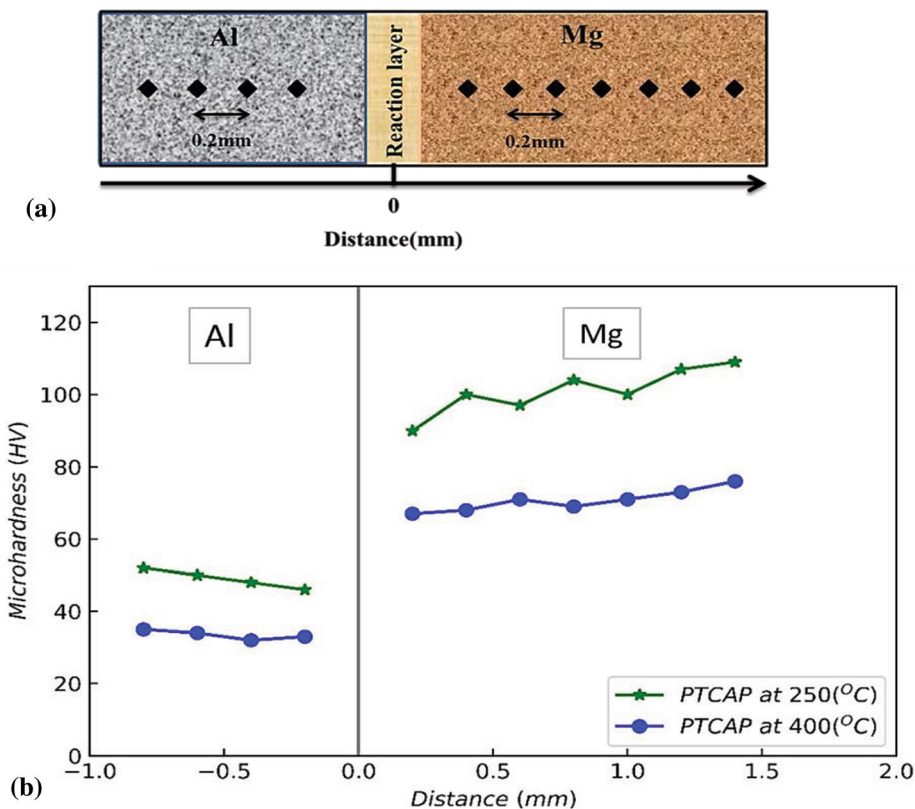


Fig. 10 (a) Schematic of microhardness points distribution and (b) microhardness distribution across the cross sections of the tubes after PTCAP processing of bilayer tube at different temperatures

tubes. The hardness values showed a slight trend toward the exterior sides due to the distribution of applied strains. However, all values were within a very narrow range, indicating a high degree of structural homogeneity in PTCAP, as shown in Fig. 10(b).

Furthermore, it can be seen that by increasing the temperature, the hardness distributions become more uniform.

Undoubtedly, the increase in the formability of Al and AM60 caused by the increase in temperature is the strongest argument for this uniform distribution. However, at temperature 250 °C, some fluctuations in the microhardness curves of AM60 are observed that with increasing temperature to 400 °C have almost disappeared (Fig. 10b). These fluctuations are feasible because of the existence of massive β -phases and some

unrefined grains, which have a larger mean grain size. This area is compared with the refined grain regions. This comparison revealed that distributed β -phase regions have a higher hardness. A similar trend in hardness distribution has been reported by Faraji et al. for AZ91 magnesium alloy after the TCAP process (Ref 30).

3.3 Interface analysis

Al 1050/AM60 bimetallic tube's interface PTCAPed at 400 °C is depicted in Fig. 11(a). The results of EDS (Table 2) for selected points in Fig. 11(a) indicate that there are two intermetallic compound layers inside the reaction layer. The intermetallic compound layers from Mg to Al are indicated as $Al_{12}Mg_{17}$ and Al_3Mg_2 . With regard to Al-Mg binary phase diagram (Ref 42), in this case, it is observable that the peak temperature is lower comparing the eutectic temperature (430 °C), and it does not reach melting conditions at the interface. This suggests that the solid-state inter-diffusion of Mg and Al atoms produces the reaction layer. The presence of these intermetallic compounds at the Al and Mg interface at high temperatures by other researchers has also been confirmed (Ref 43-45). Observations of microscopic specimens indicate the presence of intermetallic layers at temperatures of 250–400 °C and with thicknesses between 2 and 15 μm . The EDS line scan of the Mg, Al distribution across the interface of tubes at different temperatures is shown in Fig. 11(b), (c), and (d). As is seen, there has been shown only a small amount of diffusion on Al and Mg after the PTCAP process at 250 °C and the diffusion region between the Al and Mg alloy is increased by increasing the temperature up to 350 °C and then 400 °C. Indeed, the diffusion process is a phenomenon that is activated thermally, and it accelerates by increasing temperature, which results in thickening the intermetallic compounds at the interface of tubes (Fig. 12).

The optical observation shows that the thickness of the boundary layer fluctuates a lot because of the fragmentation of the primary intermetallic compounds interface layer. Actually, we can say that the primary mechanism for bonding tubes is likely due to this fragmentation. In other words, the primary intermetallic layer is formed in the first half of a PTCAP pass. Next, this intermetallic compound layer is fragmented at the start of the second half PTCAP pass when the materials are passing through the shear zone of the PTCAP mold, and after that, materials again come into contact between two fragments

and so it results in the formation of a new secondary layer. The same bonding mechanism for hydrostatic extruded Al-Mg-compound has been evaluated by Kirbach et al. (Ref 46).

Figure 12 indicates the bonding strength and average thickness of intermetallic compounds for bimetallic tubes PTCAPed at various temperatures. Here, it is worth noting that in order to minimize the impact of local fluctuations on the thickness, five measurement points at both outer edges were selected. The increased bond strength of tubes with increasing the temperature based on the observation is justifiable through this way that the thickness of the primary intermetallic compounds layers is increased in the first half of a PTCAP pass by increasing the temperature and then the thicker primary

Table 2 EDS results of selected zones specified in Fig. 11(a) (at.%)

Region of interest	Al	Si	Mn	Zn	Mg
Magnesium alloy	5.65	0.06	0.27	0.26	93.74
$Al_{12}Mg_{17}$ (layer 1)	44.7	0.07	0.25	0.24	54.74
Al_3Mg_2 (layer 2)	59.4	0.08	0.1	0.2	40.22
Aluminum alloy	99.68	0.08	0.055	0.015	0.020

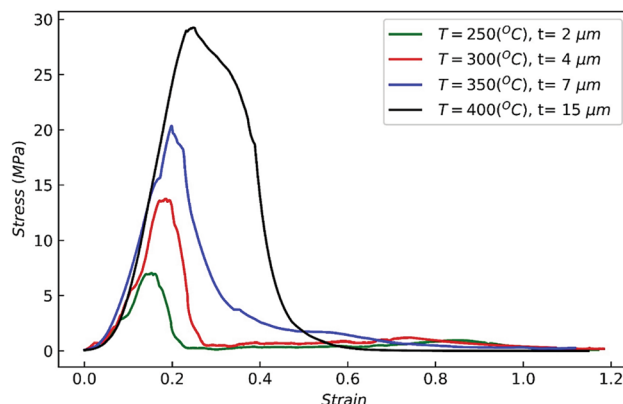


Fig. 12 Shear bonding strength graph (t is the thickness of the interface)

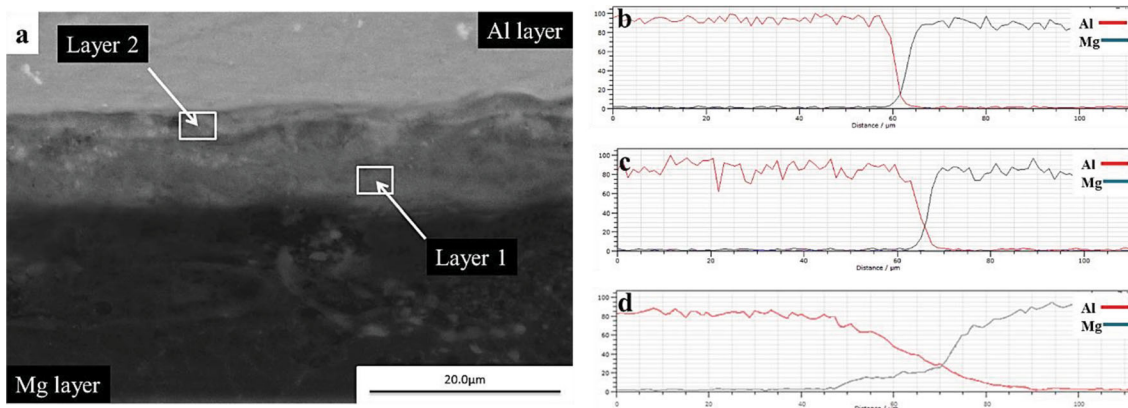


Fig. 11 (a) SEM image of the Al/Mg interface after the process at the temperature of 400 °C and EDS line scan of the Mg and Al distribution across the tube's interface after the process at (b) 250 °C, (c) 350 °C, and (d) 400 °C

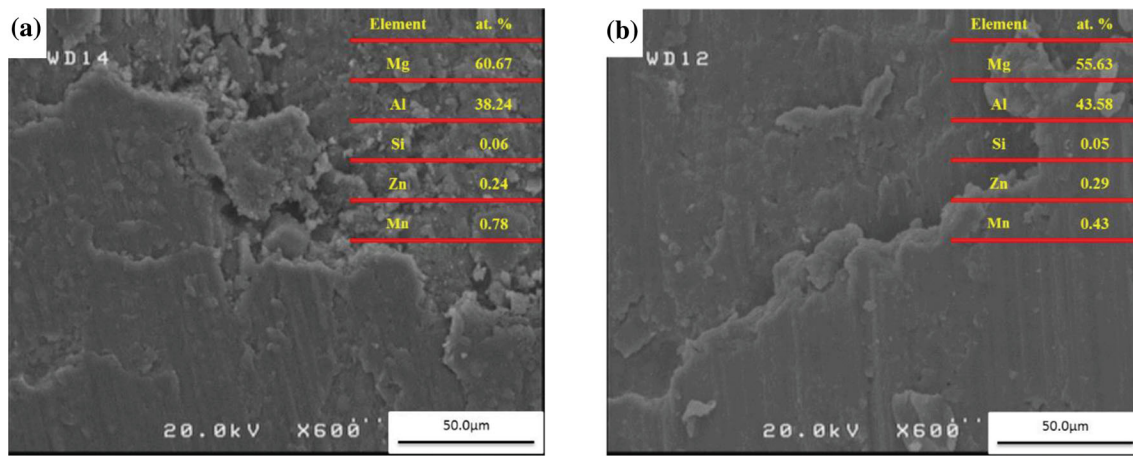


Fig. 13 SEM images of the fracture surfaces of the PTCAPed tubes at 400 °C on the (a) Mg side (b) Al side

intermetallic compounds layer results in severe fragmentation in the second half of the PTCAP pass in less strains; finally, it will produce more distance for a new secondary boundary. Besides, a stronger secondary boundary is likely to exist at higher temperatures within fragmented areas.

After separation by the shear bond test, the surfaces of the tubes were examined by SEM, and the phases were determined by EDS. After the shear bond test, in all samples, the tubes had brittle surfaces with $\text{Al}_{12}\text{Mg}_{17}$ presented on both sides of the bond interface and Al_3Mg_2 on the side bordering Al, indicating that fracture occurred along the $\text{Al}_{12}\text{Mg}_{17}$ layer. Figure 13 illustrates the fracture surfaces in the PTCAPed sample at 400 °C.

4. Conclusion

In this study, PTCAP was successfully introduced as a new approach to produce bimetallic tubes. This process consists of two half-cycles. In the first half-cycle, the tube reaches its maximum diameter, and by passing through the shear zone in the second half-cycle, the tube returns to its initial size. According to experimental results, it is proved that this process is an effective and successful method to produce the bimetallic tube, which not only provides the desired shear strength but also results in the properties of the SPD materials. The following results can be concluded:

- Dynamic recrystallization as the dominant deformation mechanism in this process causes significant grain refinement in both the pure Al and the AM60 magnesium alloy after one pass.
- The crushed precipitates could act as pinning obstacles against the grain growth of DRXed grains. By increasing PTCAP temperature ($T > 350$ °C), due to the dissolution of β -phase, the amount of pinning precipitates decreases, and the average size of the DRXed grains becomes larger.
- Remarkable grain refinement after one pass PTCAP led to a striking increase in hardness of the initial Al and AM60 tubes, which is justified by the Hall–Petch equation.
- By increasing the temperature from 250 °C up to 400 °C, the shear bond strength increased from 7 to 30 MPa, which corresponded to the increasing diffusion region be-

tween the Al and Mg alloy. For this reason, it can be said that diffusion is the major controlling mechanism of shear bond strength during this process.

- Fragmentation of the primary intermetallic layer at the start of the second half PTCAP pass and production of new binder between intact surfaces of tubes can be the main mechanisms for acceptable shear bond strength of the PTCAP technique.

Acknowledgments

This work is supported by Iran National Science Foundation (INSF).

References

1. Y.J. Kim, S.-H. Kim, J.U. Lee, J.O. Choi, H.S. Kim, Y.M. Kim, Y. Kim and S.H. Park, Effects of Cold Pre-forging on Microstructure and Tensile Properties of Extruded AZ80 Alloy, *Mater. Sci. Eng. A*, 2017, **708**, p 405–410.
2. Z. Jiang, Z. Fan, W. Jiang, G. Li, Y. Wu, F. Guan and H. Jiang, Interfacial Microstructures and Mechanical Properties of Mg/Al Bimetal Produced by a Novel Liquid–Liquid Compound Casting Process, *J. Mater. Process. Technol.*, 2018, **261**, p 149–158.
3. S. Amani, G. Faraji, H.K. Mehrabadi, K. Abrinia and H. Ghanbari, A Combined Method for Producing High Strength and Ductility Magnesium Microtubes for Biodegradable Vascular Stents Application, *J. Alloys Compd.*, 2017, **723**, p 467–476.
4. B. Carcel, J. Sampedro, A. Ruescas and X. Toneu, Corrosion and Wear Resistance Improvement of Magnesium Alloys by Laser Cladding with Al-Si, *Phys. Procedia*, 2011, **12**, p 353–363.
5. G. Faraji and H.S. Kim, Review of Principles and Methods of Severe Plastic Deformation for Producing Ultrafine-grained Tubes, *Mater. Sci. Technol.*, 2017, **33**, p 905–923.
6. M. Paramsothy, N. Srikanth and M. Gupta, Solidification Processed Mg/Al Bimetal Macrocomposite: Microstructure and Mechanical Properties, *J. Alloys Compd.*, 2008, **461**(1–2), p 200–208.
7. A. Wang, S. Sircar and J. Mazumder, Laser Cladding of Mg–Al Alloys, *J. Mater. Sci.*, 1993, **28**(19), p 5113–5122.
8. S. Mróz, A. Gontarz, K. Drozdowski, H. Bala and P. Szota, Forging of Mg/Al Bimetallic Handle Using Explosive Welded Feedstock, *Arch. Civ. Mech. Eng.*, 2018, **18**, p 401–412.
9. G.P. Chaudhari and V. Acoff, Cold Roll Bonding of Multi-layered Bi-metal Laminate Composites, *Compos. Sci. Technol.*, 2009, **69**(10), p 1667–1675.

10. L. Zhao and Z. Zhang, Effect of Zn Alloy Interlayer on Interface Microstructure and Strength of Diffusion-Bonded Mg–Al joints, *Scr. Mater.*, 2008, **58**(4), p 283–286.
11. D. Rozumek and R. Bański, Crack Growth Rate Under Cyclic Bending in the Explosively Welded Steel/Titanium Bimetals, *Mater. Des.*, 2012, **38**, p 139–146.
12. M. Roostaei and R. Darabi, Investigation on Formability of Three-Layer Joined Al/Cu/Al Sheets Annealed at Different Temperature, *Mater. Sci. Technol.*, 2020, **36**(13), p 1476–1486.
13. Y.S. Sato, S.H.C. Park, M. Michiuchi and H. Kokawa, Constitutional Liquation During Dissimilar Friction Stir Welding of Al and Mg Alloys, *Scr. Mater.*, 2004, **50**(9), p 1233–1236.
14. J. Yan, Z. Xu, Z. Li, L. Li and S. Yang, Microstructure Characteristics and Performance of Dissimilar Welds Between Magnesium Alloy and Aluminum Formed by Friction Stirring, *Scr. Mater.*, 2005, **53**(5), p 585–589.
15. Q. Wang, Y. Song, B. Jiang, J. Fu, A. Tang, H. Sheng, J. Song, D. Zhang, Z. Jiang and G. Huang, Fabrication of Mg/Mg Composite with Sleeve-Core Structure and Its Effect on Room-Temperature Yield Asymmetry via Bimetal Casting-Co-extrusion, *Mater. Sci. Eng. A*, 2020, **769**, p 138476.
16. C. Ji, H. Huang, J. Zhang and R. Zhao, Influence of the Substrate Strip on the Asymmetric Heat Transfer of Twin-Roll Casting for Fabricating Bimetallic Clad Strips, *Appl. Therm. Eng.*, 2019, **158**, p 113818.
17. E. Hajjari, M. Divandari, S. Razavi, S. Emami, T. Homma and S. Kamado, Dissimilar Joining of Al/Mg Light Metals by Compound Casting Process, *J. Mater. Sci.*, 2011, **46**(20), p 6491–6499.
18. R. Mola, T. Bucki and A. Dziadoń, Formation of Al-Alloyed Layer on Magnesium with Use of Casting Techniques, *Arch. Foundry Eng.*, 2016, **16**, p 112–116.
19. B. Zhu, W. Liang and X. Li, Interfacial Microstructure, Bonding Strength and Fracture of Magnesium–Aluminum Laminated Composite Plates Fabricated by Direct Hot Pressing, *Mater. Sci. Eng. A*, 2011, **528**(21), p 6584–6588.
20. H. Matsumoto, S. Watanabe and S. Hanada, Fabrication of Pure Al/Mg–Li Alloy Clad Plate and Its Mechanical Properties, *J. Mater. Process. Technol.*, 2005, **169**(1), p 9–15.
21. M. Mehrzad, A. Sadeghi and M. Farahani, Microstructure and Properties of Transient Liquid Phase Bonding of AM60 Mg Alloy to 304 Stainless Steel with Zn Interlayer, *J. Mater. Process. Technol.*, 2019, **266**, p 558–568.
22. K. Wu, H. Chang, E. Maawad, W. Gan, H. Brokmeier and M. Zheng, Microstructure and Mechanical Properties of the Mg/Al Laminated Composite Fabricated by Accumulative Roll Bonding (ARB), *Mater. Sci. Eng. A*, 2010, **527**(13–14), p 3073–3078.
23. G. Faraji and H. Torabzadeh, An Overview on the Continuous Severe Plastic Deformation Methods, *Mater. Trans.*, 2019, **60**(7), p 1316–1330.
24. R. Lapovok, H.P. Ng, D. Tomus and Y. Estrin, Bimetallic Copper–Aluminum Tube by Severe Plastic Deformation, *Scr. Mater.*, 2012, **66**(12), p 1081–1084.
25. Y. Tian, H. Hu and D. Zhang, A Novel Severe Plastic Deformation Method for Manufacturing Al/Mg bimetallic Tube, *Mater. Manuf. Process.*, 2021, **30**, p 1256–1261.
26. S. Ghadimi, M. Sedighi, F. Djevanroodi and A. Asgari, Experimental and Numerical Investigation of a Cu–Al Bimetallic Tube Produced by ECAP, *Mater. Manuf. Process.*, 2015, **30**(10), p 1256–1261.
27. M.R. Standley and M. Knezevic, Towards Manufacturing of Ultrafine-Laminated Structures in Metallic Tubes by Accumulative Extrusion Bonding, *Metals*, 2021, **11**(3), p 389.
28. G. Faraji, A. Babaei, M.M. Mashhadi and K. Abrinia, Parallel Tubular Channel Angular Pressing (PCAP) as a New Severe Plastic Deformation Method for Cylindrical Tubes, *Mater. Lett.*, 2012, **77**, p 82–85.
29. G. Faraji, H.S. Kim and H.T. Kashi, *Severe Plastic Deformation: Methods, Processing and Properties*, Elsevier, Amsterdam, 2018.
30. G. Faraji, M.M. Mashhadi and H.S. Kim, Tubular Channel Angular Pressing (TCAP) as a Novel Severe Plastic Deformation Method for Cylindrical Tubes, *Mater. Lett.*, 2011, **65**(19–20), p 3009–3012.
31. M. Mesbah, F. Fadaeifard, A. Karimzadeh, B. Nasiri-Tabrizi, A. Rafieerad, G. Faraji and A. Bushroa, Nano-mechanical Properties and Microstructure of UFG Brass Tubes Processed by Parallel Tubular Channel Angular Pressing, *Metals Mater. Int.*, 2016, **22**(6), p 1098–1107.
32. M. Javidikia and R. Hashemi, Mechanical Anisotropy in Ultra-Fine Grained Aluminium Tubes Processed by Parallel-Tubular-Channel Angular Pressing, *Mater. Sci. Technol.*, 2017, **33**(18), p 2265–2273.
33. V. Tavakkoli, M. Afrasiab, G. Faraji and M. Mashhadi, Severe Mechanical Anisotropy of High-Strength Ultrafine Grained Cu–Zn Tubes Processed by Parallel Tubular Channel Angular Pressing (PTCAP), *Mater. Sci. Eng. A*, 2015, **625**, p 50–55.
34. M.T. Pérez-Prado, J. Del Valle, J. Contreras and O.A. Ruano, Microstructural Evolution During Large Strain Hot Rolling of an AM60 Mg Alloy, *Scr. Mater.*, 2004, **50**(5), p 661–665.
35. A. Feng and Z. Ma, Enhanced Mechanical Properties of Mg–Al–Zn Cast Alloy via Friction Stir Processing, *Scr. Mater.*, 2007, **56**(5), p 397–400.
36. H. Mirzadeh, M. Roostaei, M. Parsa and R. Mahmudi, Rate Controlling Mechanisms During Hot Deformation of Mg–3Gd–1Zn Magnesium Alloy: Dislocation Glide and Climb, Dynamic Recrystallization, and Mechanical Twinning, *Mater. Des.*, 2015, **68**, p 228–231.
37. M. Roostaei, M. Parsa, R. Mahmudi and H. Mirzadeh, Hot Compression Behavior of GZ31 Magnesium Alloy, *J. Alloys Compd.*, 2015, **631**, p 1–6.
38. T. Al-Samman and G. Gottstein, Dynamic Recrystallization During High Temperature Deformation of Magnesium, *Mater. Sci. Eng. A*, 2008, **490**(1–2), p 411–420.
39. Z. Zhao, Q. Chen, Z. Tang and C. Hu, Microstructural Evolution and Tensile Mechanical Properties of AM60B Magnesium Alloy Prepared by the SIMA Route, *J. Alloys Compd.*, 2010, **497**(1–2), p 402–411.
40. H. Yu, Y. Xin, M. Wang and Q. Liu, Hall–Petch Relationship in Mg alloys: A Review, *J. Mater. Sci. Technol.*, 2018, **34**(2), p 248–256.
41. C.J. Luis, J. León, R. Luri, I. Puertas, I. Pérez and D. Salcedo, Development of Nano-structured AA1050 by ECAE and Thermal Treatments, *Soft Nanosci. Lett.*, 2011, **1**(4), p 120–129.
42. S.H. Treating, *ASM Handbook W* (2013)
43. D. Dietrich, D. Nickel, M. Krause, T. Lampke, M. Coleman and V. Randle, Formation of Intermetallic Phases in Diffusion-Welded Joints of Aluminium and Magnesium Alloys, *J. Mater. Sci.*, 2011, **46**(2), p 357–364.
44. J. Wang, Y. Li, P. Liu and H. Geng, Microstructure and XRD Analysis in the Interface Zone of Mg/Al Diffusion Bonding, *J. Mater. Process. Technol.*, 2008, **205**(1–3), p 146–150.
45. S. Amani and G. Faraji, Processing and Properties of Biodegradable Magnesium Microtubes for Using as Vascular Stents: A Brief Review, *Met. Mater. Int.*, 2019, **25**(5), p 1341–1359.
46. C. Kirbach, M. Stockmann and J. Ihlemann, A Fragmentation Criterion for the Interface of a Hydrostatic Extruded Al-Mg-Compound, *Metals*, 2018, **8**(3), p 157.

Publisher's Note Springer Nature remains neutral with regard to jurisdictional claims in published maps and institutional affiliations.